Semiannual Progress Report

437

Submitted to:	National Aeronautics and Space Adminstration Langley Research Center Hampton, Va 23665
Institution:	Hampton University Dept of Physics and Engineering
Title of Research:	Direct Solar-Pumped Iodine Laser Amplifier
NASA Grant Number	NAG-1-441
Period Covered	March 1, 1987 - Sept. 30, 1987
Principal Investigator	Dr. Kwang S. Han
Research Associates	Dr. K. H. Kim Mr. L. V. Stock

Direct Solar-Pumped Iodine Laser Amplifier

Contents

Abstract

This semiannual progress report covers the period from March 1, 1987 to September 30, 1987 under NASA grant NAG-1-441 entitled "Direct solar-pumped iodine laser amplifier". During this period Nd:YAG and Nd:Cr:GSGG crystals have been tested for the solar-simulator pumped cw laser, and loss mechanisms of the laser output power in a flashlamp-pumped iodine laser have been also identified theoretically.

It was observed that the threshold pump-beam intensities for both Nd:YAG and Nd:Cr:GSGG crystals were about 1,000 solar constants, and the cw laser operation of the Nd:Cr:GSGG crystal was more dificult than that of the Nd:YAG crystal under the solar-simulator pumping. The possibility of the Nd:Cr:GSGG laser operation with a fast continuously chopped pumping was also observed. In addition, good agreement between the theorecal calculations and the experimental data on the loss mechanisms of a flashlamp-pumped iodine laser at various fill pressures and various lasants was achieved.

Evalution of Solid State Laser Materials for Solar Pumping

A. Introduction

Study on the evalution of various laser crystals for high power solar-pumped laser has been continued during this report period. In the previous semiannual report[Ref.1] literature survey on material charateristics and lasing efficiencies of various solid state laser crystals, such as Ruby, Nd:YAG, Nd:Glass, Nd:Cr:GSGG, Nd:YLF, Alexandrite and Emerald, has been reported. In addition, theoretical calculations for solar-beam absorption by each crystal at various concentrations and rod diameters, and for temperature distribution within laser crystal rods with various cooling water flowrates, have been also given in the report. Experimental work on the solar-simulator pumped Nd:YAG and Nd:Cr:GSGG crystals has been performed during this current period. The measured threshold of a 1/8"-diameter x 3"-long Nd:YAG crystal with coupling mirrors, one with maximum reflectance and 0.3m curvature and the other one with reflectance of 98% and 0.3-m curvature, was about 200A of the solar-simulator input curent which corresponds to the beam intensity of about 1,000 solar constants at the focus of a conical collector of 16.6-cm diameter, and the measured peak laser power was about 320mW at the solar-simulator input current of 700A.

The cw laser operation of Nd:Cr:GSGG was more difficult than Nd:YAG possibly because of its high absorption of the solar-simulator beam and relatively low thermal conductivity. The same result was found recently in published papers[Refs. 2 and 3]. With a continuous solar-simulator pumping lasing of the Nd:Cr:GSGG crystal lasted only about 3 seconds. However, with a chopped pumping its chopped lasing lasted more than 3 minutes which can be extended to forever with using a proper chopper material. the chopper's open-to-closed ratio used in the above test was one. The peak laser power achieved with a 1/8" didameter x 2.94" long Nd:Cr:GSGG crystal was about 400mW which could be increased with an optimum resonator coupling.

The longest cw lasing period observed with the Nd:YAG crystal without a direct mirror coating was 17 seconds. But the lasing was unstable and not

repeatable in the following runs because of the optical misalignment caused by thermal effect. A stable laser operation longer than that is desired in order to have accurate power measurements and to collect comparative data among various laser crystals. The choice of a right kind of lasing material is very important to reach our goal which is a high power cw laser achievement. Two different kinds of solar-simulator beam collector, which are a conical type collector and a rectangular-type mirror cavity collector with two open ends on the opposite sides, have been also tested. The experimental setups and results with the conical type and the rectangular mirror-cavity type of the solar-simulator collectors will be discussed in the following sections.

B. Experiments and Results

The experimental setup with a conical type collector for solar-simulator pumped solid state lasers is shown in Fig. 1. Dimensions of the conical collector and the detailed diagram of the laser crystal holder and cooling water jacket were reported in the previous semiannual progress report. The laser crystal size was of 1/8"-diameter and 3"-long, and the inner diameter of the cooling jacket was 13mm. The mirror M1 has a reflectivity of greater than 99.5% at λ=1.06um and a curvature of 0.3m. The reflectivity of the output mirror M2 is supposed to be changed to several values for the maximum laser output. The detectors used to measure the pumping light and the laser output signal were EG&G silicon photodiodes and were connected to a bias voltage of -90 V.

The first observed laser signal of a Nd:YAG crystal with the solar-simulator input current of 200A is shown in Fig.2. The reflectivity of the output mirror used was 98% and its curvature was 0.3 m. The coolent flowrate was 1.5 gallons per minute. About 17 second laser operation which is shown in Fig. 3 was achieved with the same experimental setup and the solar-simulator input current of 400A. However, the system was very sensitive to the thermal effect. The alignment of the laser cavity was changed by heat from the solar-simulator beam while the system was lasing, and then it stoped lasing before the pumping was ended. Furthermore, the alignment was also changed gradually by each operation, and the lasing period became shorter and shorter during consecutive operations as shown in Figs. 3 through 5. The alignment did not come back to the original condition for the most time even after the system was cooled down.

The measured laser powers of the Nd:YAG crystal are shown in Figs. 6 and 7 as a function of the solar-simulator's input current and as a function of the solar-simulator's beam intensity at the crystal surface in a unit of solar constant, respectively. The silicon photodiode, which was used to measure the

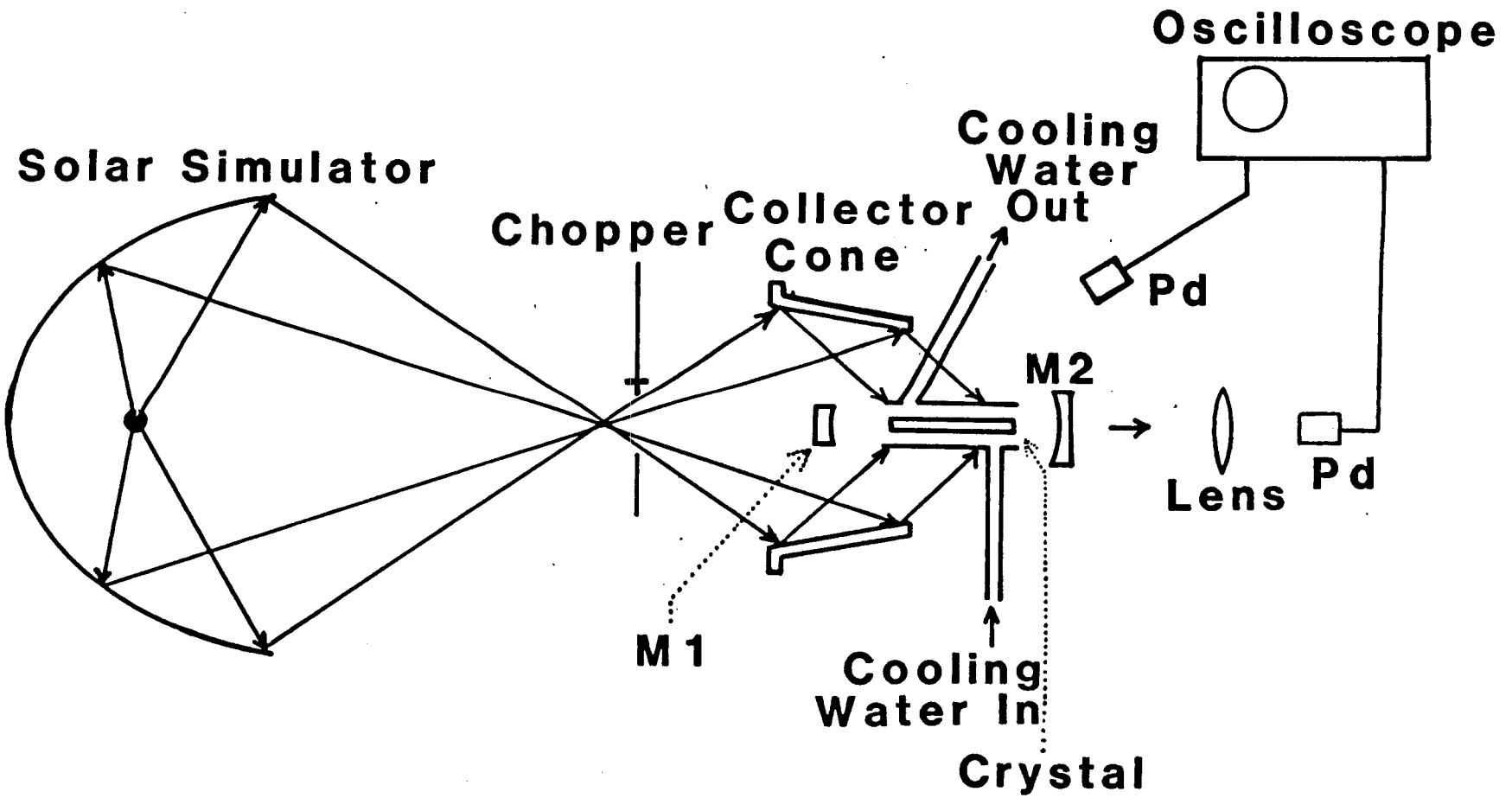

Figure 1. Set-up used for the solar-simulator pumped solid state laser experiments with a conical type solar-simulator. M:mirror, Pd:silicon photodiode.

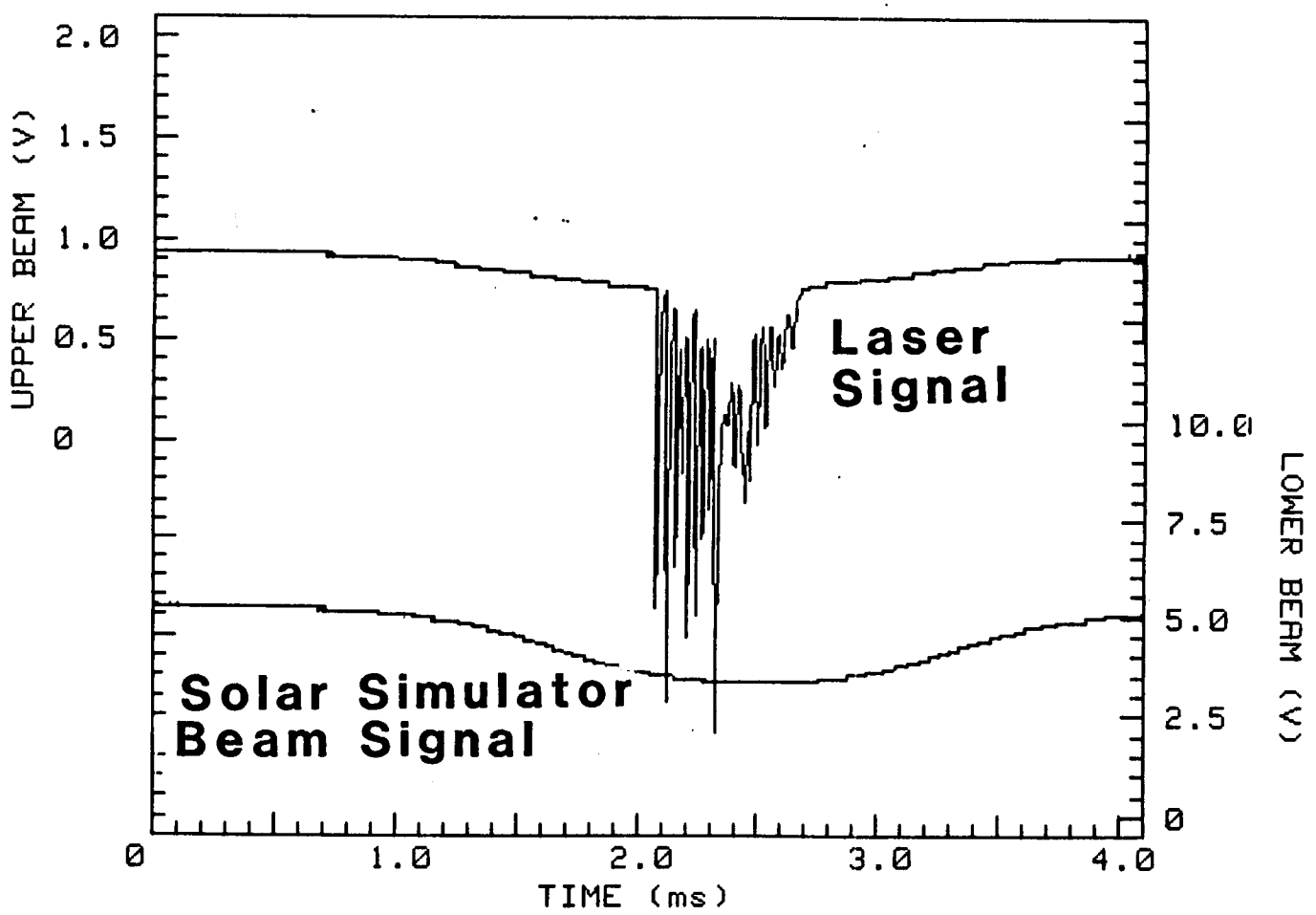

Figure 2. The first observed laser signal of a 1/8"-diameter x 3"-long Nd;YAG crystal pumped by the Tarmrack solar-simulator with the input current of 200A.

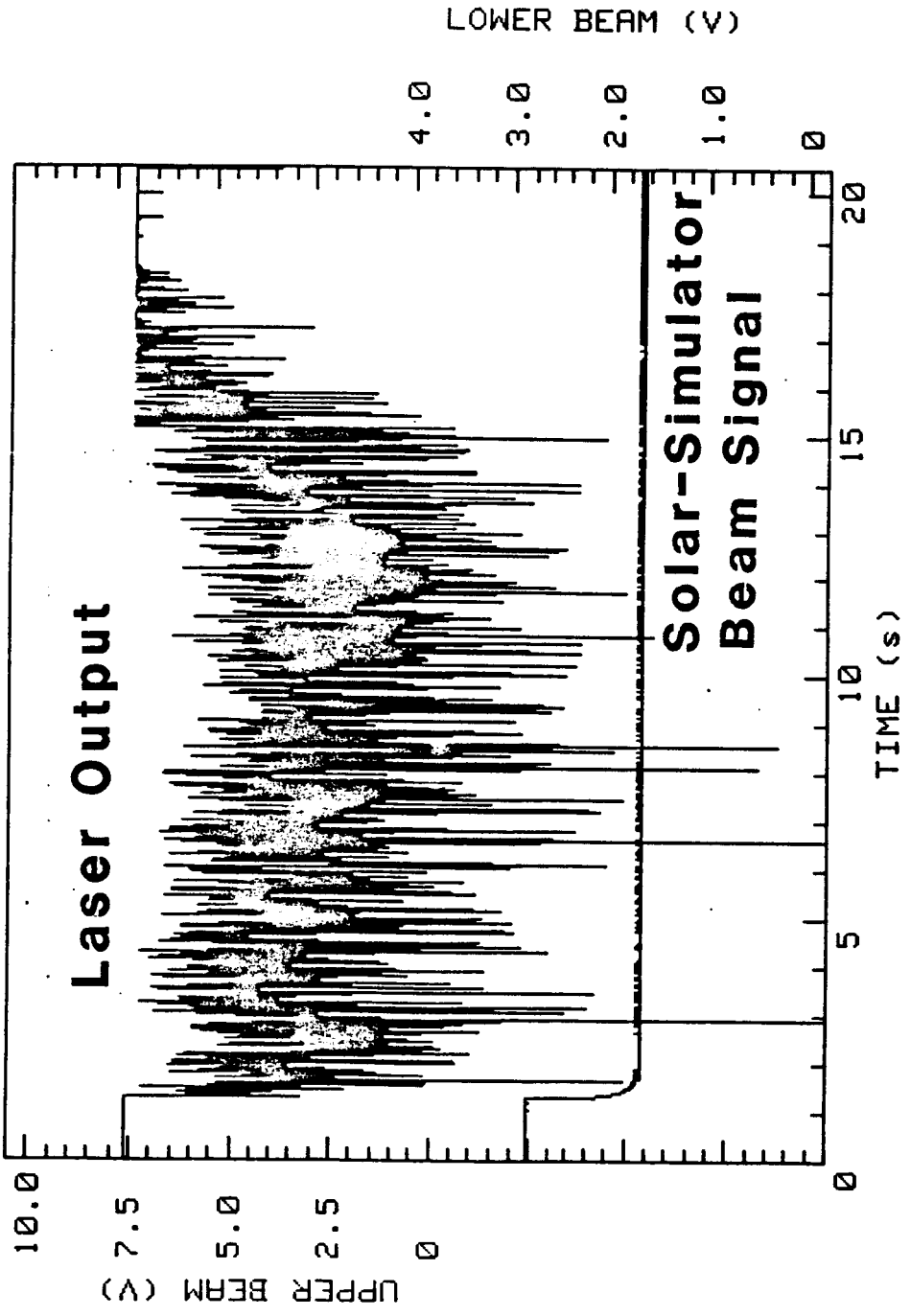

Figure 3. The Nd:YAG laser output and solar-simulator beam signals observed for a long-time operation.

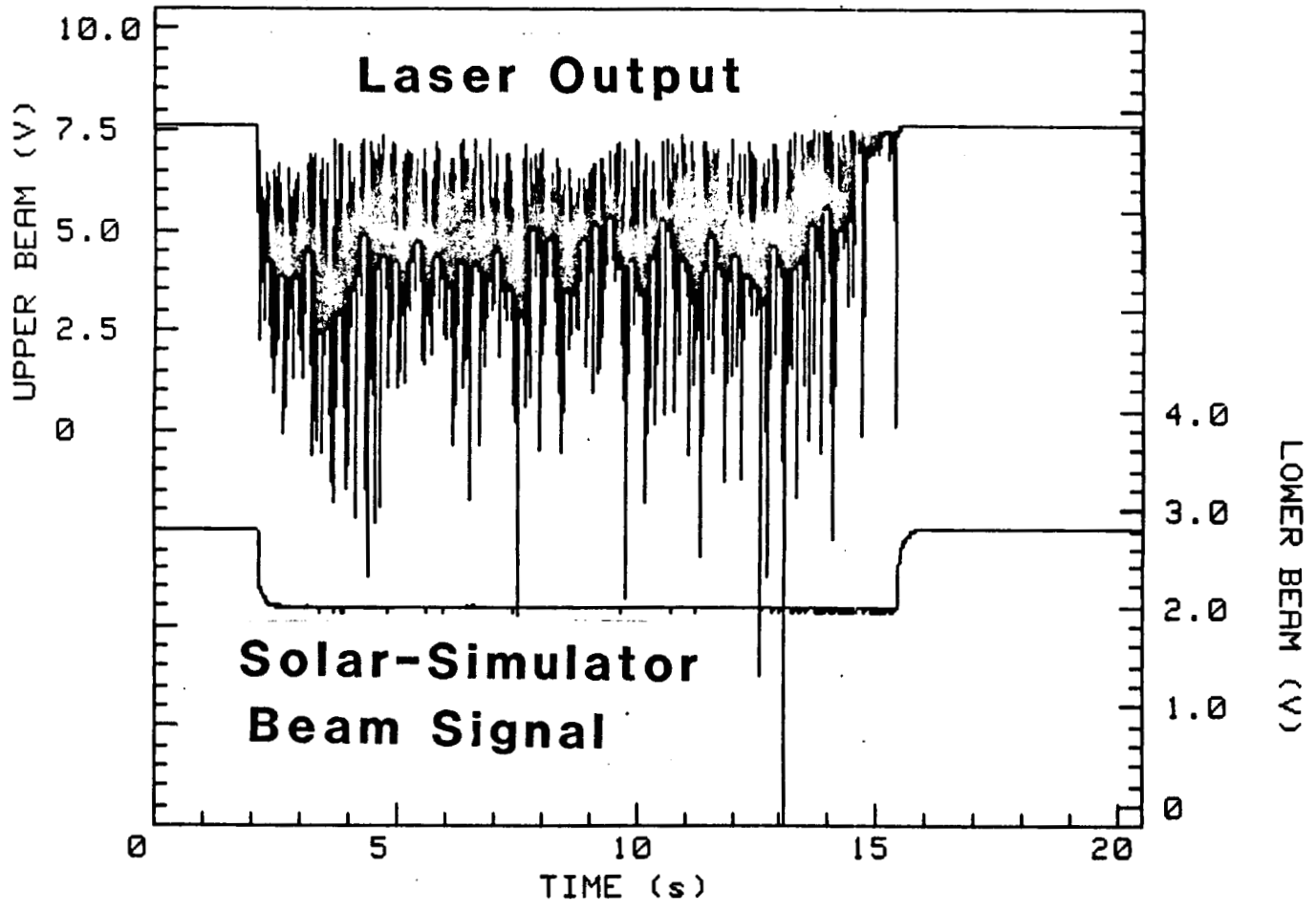

Figure 4. The Nd:YAG laser output and solar-simulator beam signals obsered in the following run after the one whose data is shown in Fig. 3.

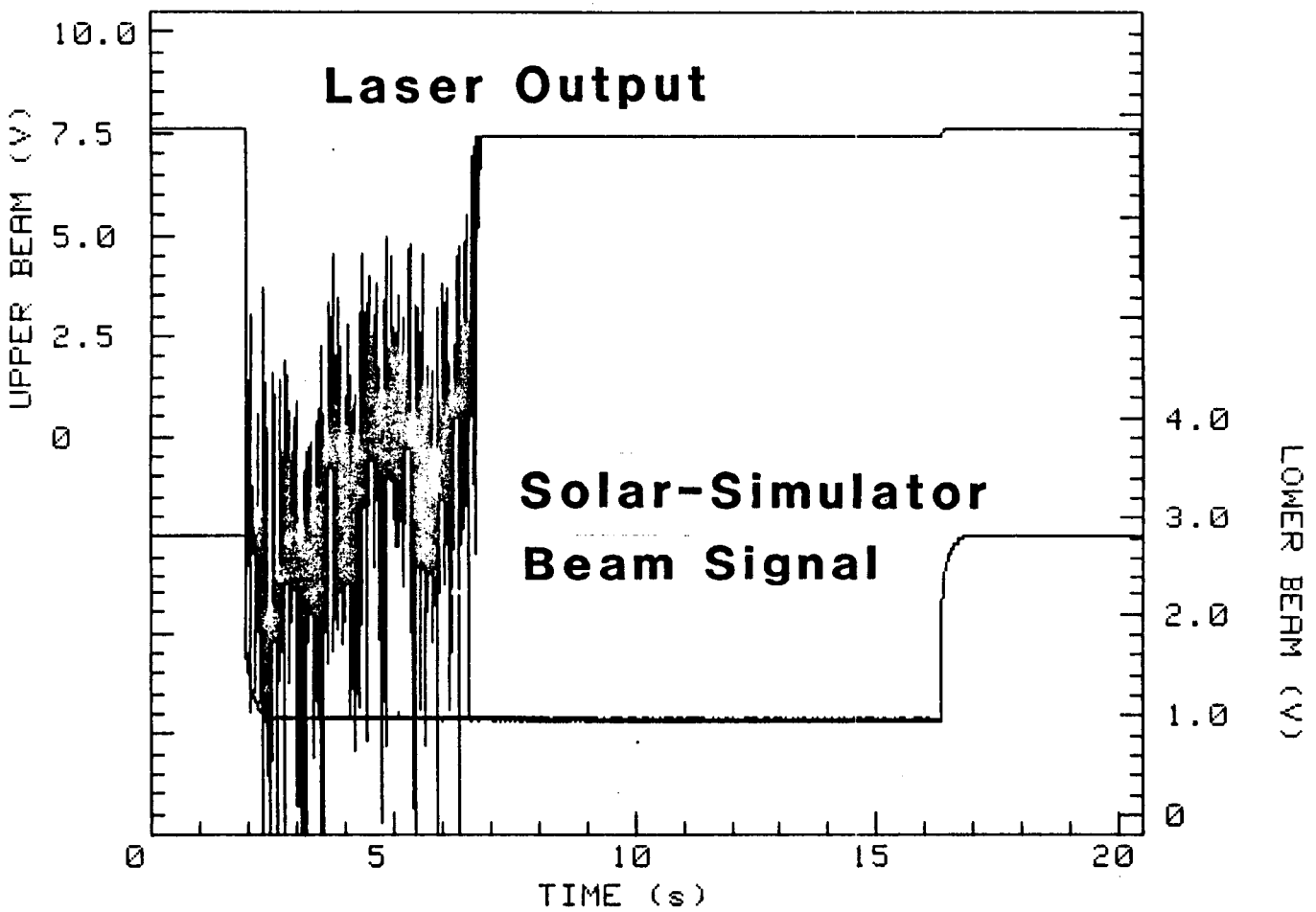

Figure 5. The Nd:YAG laser and solar-simulator beam signals observed in following run after the one whose date is shown in Fig. 4. The lasing disappears very early, possibly because of the optical misalignment caused by the thermal effect.

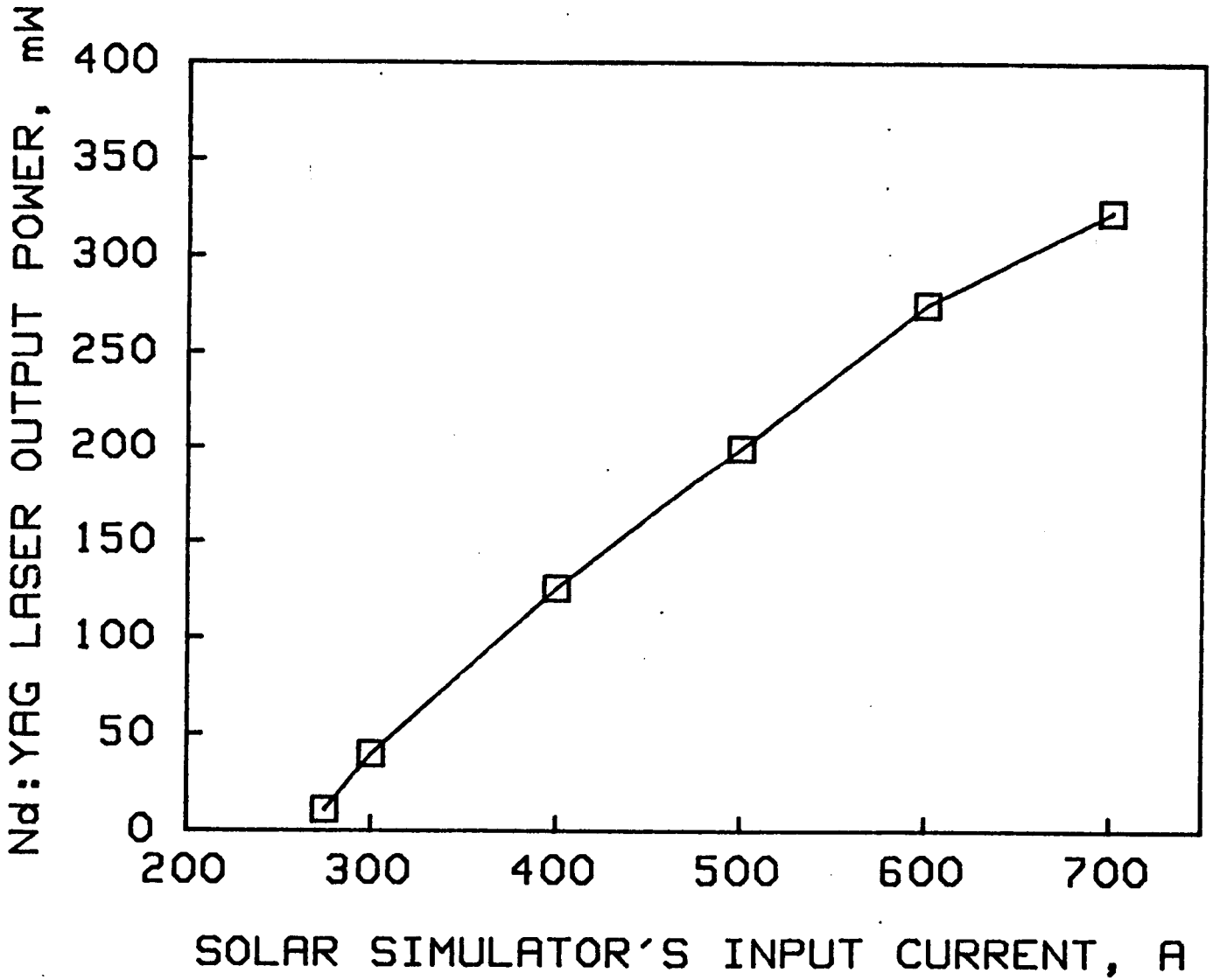

Figure 6. The Nd:YAG laser output power as a function of the solar-simulator's input currents. The Nd:YAG laser rod had a size of 1/8" diameter and 3" long, and antireflection coatings on the both ends. Coupling mirrors: R1 > 99.5% and R2 =98% and both mirrors have radius of curvature of 0.3m.

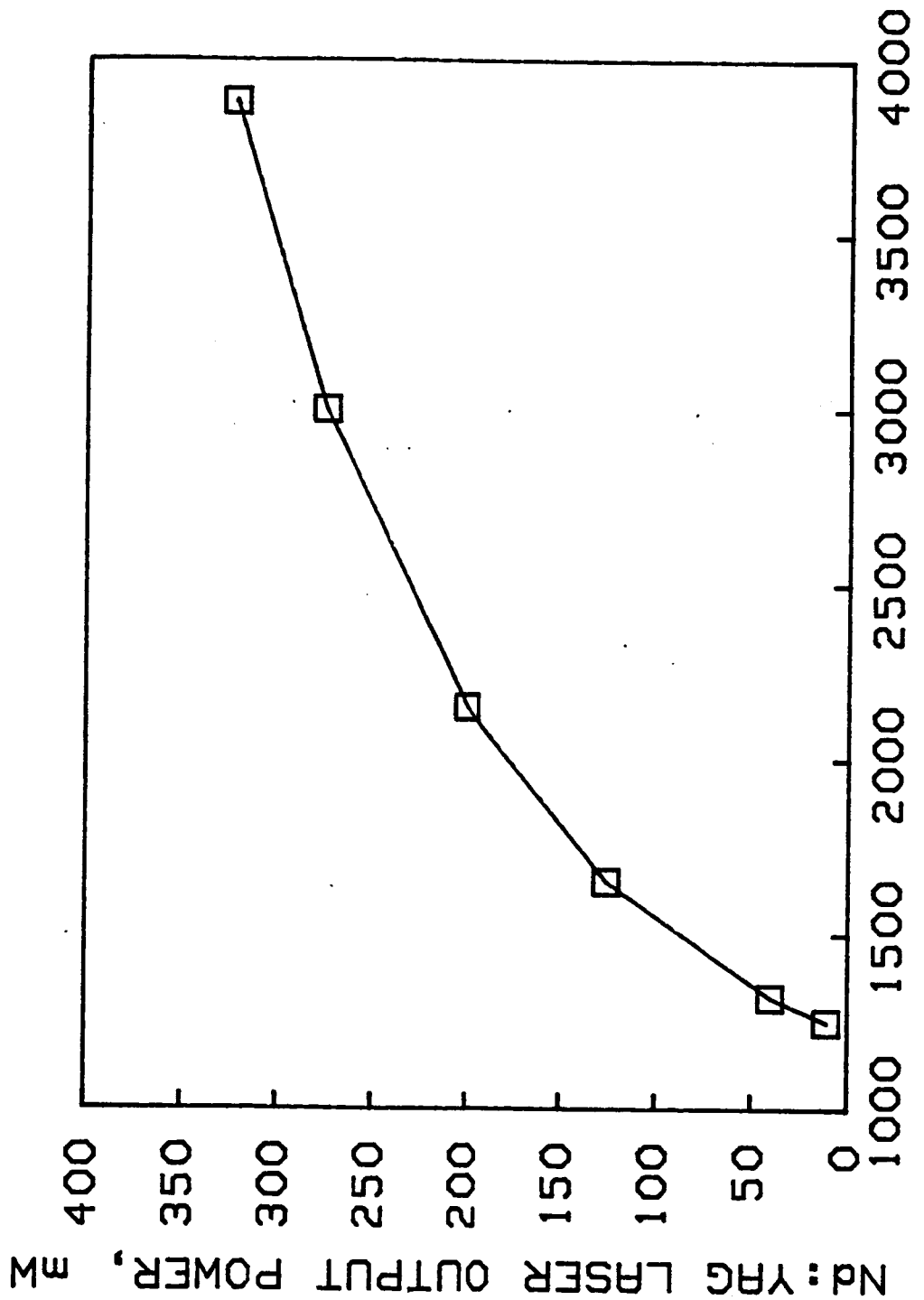

Figure 7. The Nd:YAG laser output power as a function of the solar-simulator's beam intensity at the crystal surface.

laser signal in Fig. 1, was just replaced with a Scientek thermopile power detector (model no. 360201). The detector aperture size was 2 inches and connected to a meter unit (Scientek model 36-5002). The distance between the powermeter detector and the output mirror was kept large (= 2.5m) in order to reduce the error due to the fluorescence beam which was eventually measured and taken into account for the laser power. The laser power shows the linear dependence on the solar- simulator input current, but slightly saturates at above 600A. On the other hand, the dependence of the laser power on the pump beam intensity is rather close to exponential shape. The maximum power observed was about 320mW at 700A of the solar-simulator input current.

In order to avoid the thermal problem, two different system geometries were introduced. The first one was to have a curved maximum-reflective mirror coated at one end of the laser crystal, because the system shown in Fig.1 has the highly reflective mirror and its holder exposed in the incoming solar-simulator beam. The second one was to use a different type of solar-simulator beam collector other than the conical collector. The new type of collector will be discussed later.

Figures 8 through 10 show the observed laser signals of the Nd:Cr:GSGG crystal with the solar-simulator pumping. The upper trace indicates the laser signals and the lower trace indicates the solar-simulator beam signals. The same laser system geometry as shown in Fig.1 was used except a direct mirror coating at one end of the crystal. The reflecivity of the mirror coating was greater than 99.5% and its curvature was 5m. The laser signal observed with a continuous pumping is shown in Fig. 8. The lasing lasted only about 3 seconds and a few spikes of the laser signals appeared after the first cease. This shows that the cw laser operation of the Nd:Cr:GSGG crystal may not be possible.

Fig. 9 shows the laser signals of the Nd:Cr:GSGG crystal with a chopped pumping. It is noticable that the intensity of the laser signal decreased within each chopper-open period, but the average intensity of each pulse does not change very much in the following consecutive pulses. Data on 3-minute

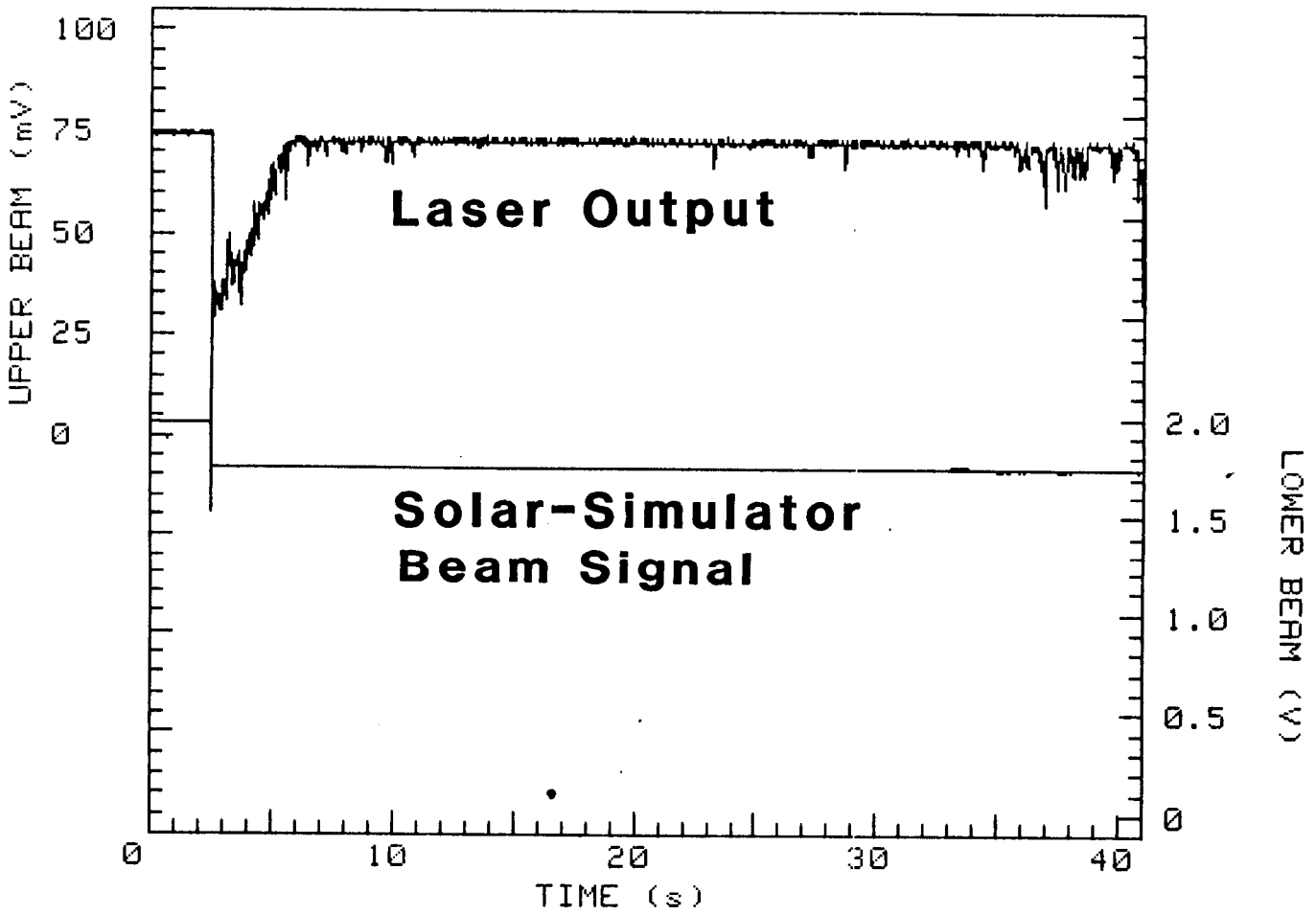

Figure 8. The Nd:Cr:GSGG laser output and solar-simulator beam signals observed during a single long-time pumping. The laser rod had a size of 1/8" diameter and 2.96" long, and the maximum reflective mirror coating at one end.

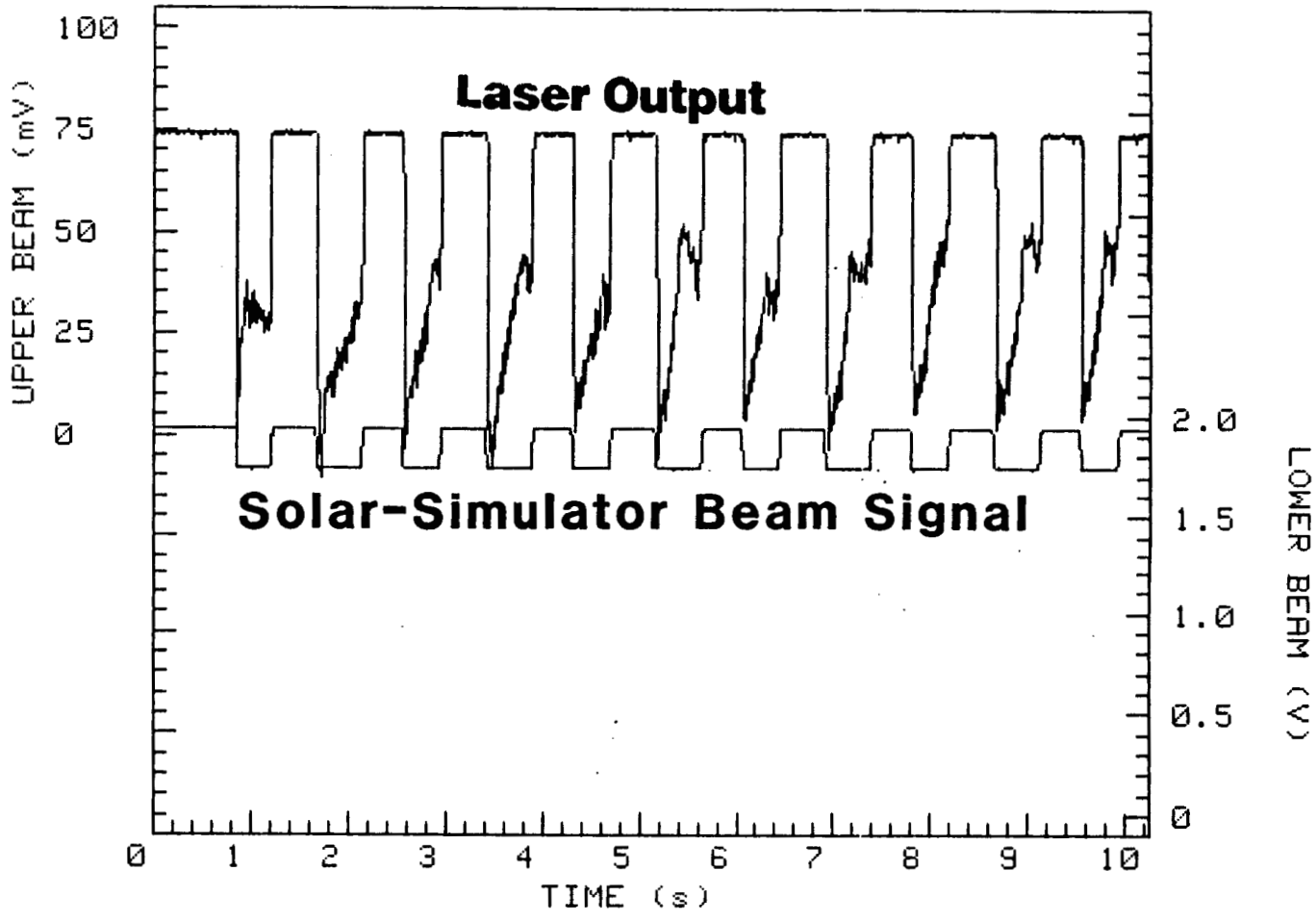

Figure 9. The observed Nd:Cr:GSGG laser output and solar-simulator's beam signals with a chopped pumping.

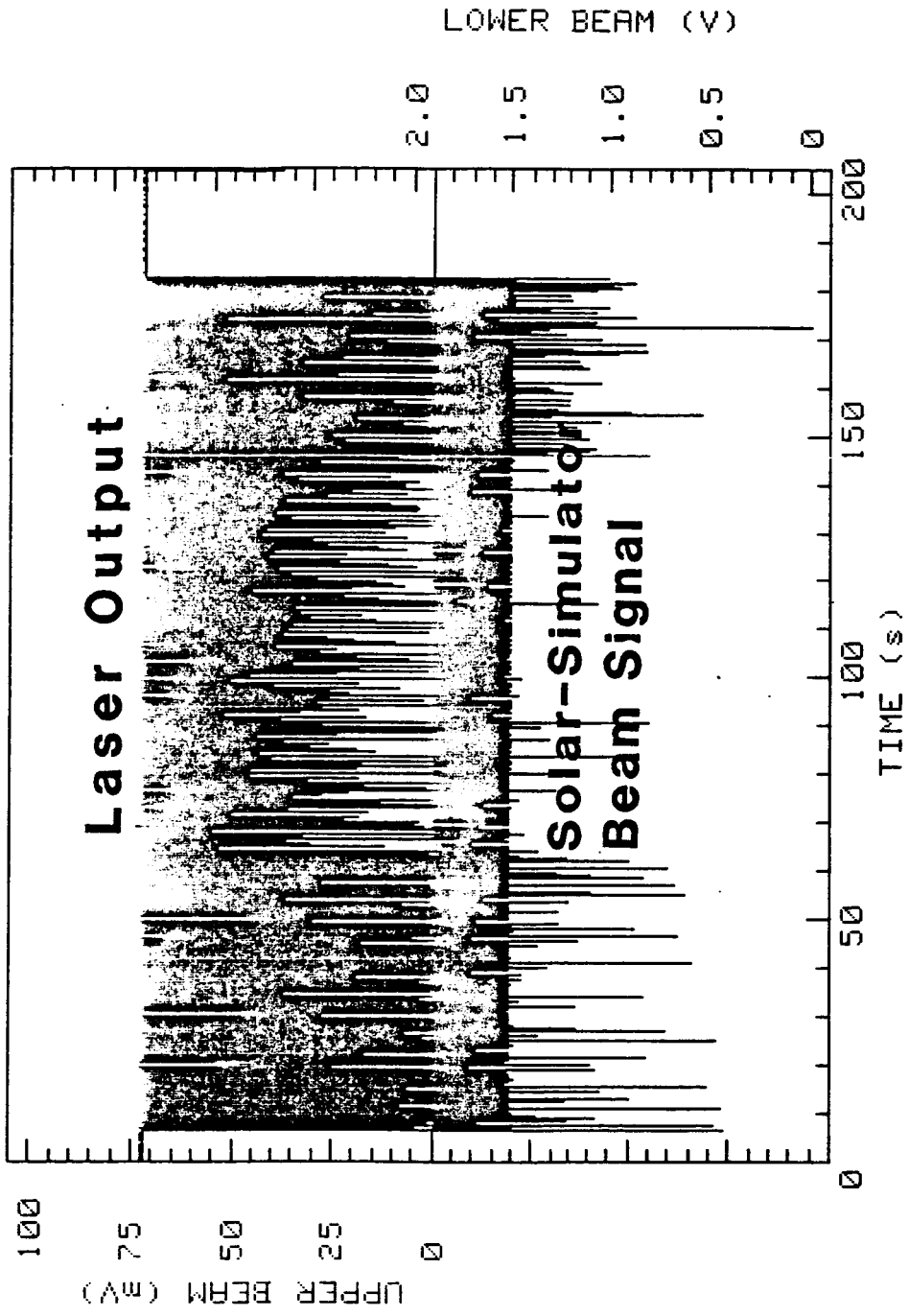

Figure 10. The observed Nd:Cr:GSGG laser output and solar-simulator's beam signals with a long-time chopped pumping.

laser operation with the use of the chopper is shown in Fig. 10. The continuously chopped lasing of the Nd:Cr:GSGG crystal could be extended longer using a proper chopper material. The maximum chopper openning size and maximum chopper speed for the continuously chopped laser operation will be determined in the following research period as well as average laser power measurement and comparison with other crystals.

Fig. 11 shows the peak laser power of the Nd:Cr:GSGG crystal, whose size is 1/8"dia. x 2.94" long, of each chopped pulse as a function of the solar-simulator's input current. This data was obtained before an optimum condition for the laser resonator has been established. It is expected that the laser power can be increased by optimizing the resonator condition which will be experimented in the following project period.

Experimental setup with a new solar-simulator beam collector is shown in Fig.12. The new solar-simulator beam collector was a rectangular-type mirror cavity with openings at two opposite ends so that the solar-simulator beam enters at one end, reflects from inner surfaces of the cavity, and leaves at the other end where the laser crystal is to be placed. The detailed shape and dimension of the mirror cavity are shown in Fig. 13. The front of the mirror cavity was placed at the solar-simulator beam focus which was located within the distance of 1.0cm from the aluminum shield board in front of the solar-simulator..

Fig.14 shows the experimental setup for the intensity distribution measurement of the solar-simulator's beam at the back of the mirror cavity. As shown in the Figure, a 45 -diffused reflector made of a 4.5-mm diameter taflon rod was placed inside an aluminum tube of a 1/4" O.D. with a fiber-optics at the other end. A small hole was made on the aluminum tube just in front of the taflon reflector to allow the beam intensity measurement only at the given position. The beam reflected from the diffused surface was sent to the spectrograph (Jarrell-Ash Monospec 27, model 82-498 with a 150 gr/mm grating) through the fiber-optics, and its spectral intensity distribution was measured by the optical multichannel analyzer (Tracor-Northern TN-6500 with a TN-6132 detector).

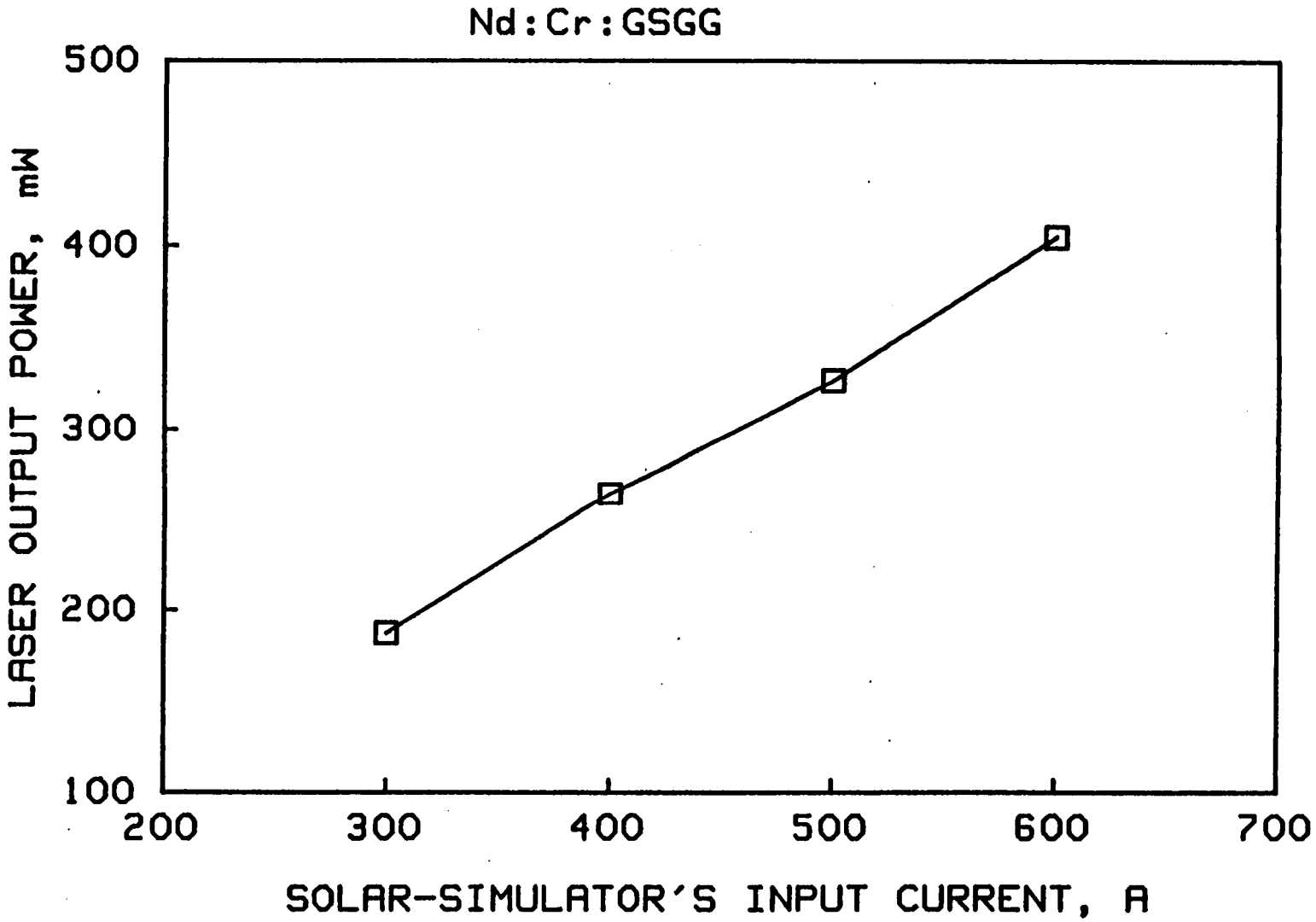

Figure 11. The observed Nd:Cr:GSGG laser output power as a function of the solar-simulator's input current. The experimental setup with the conical-type solar-simulator's beam collector was used in this measurement.

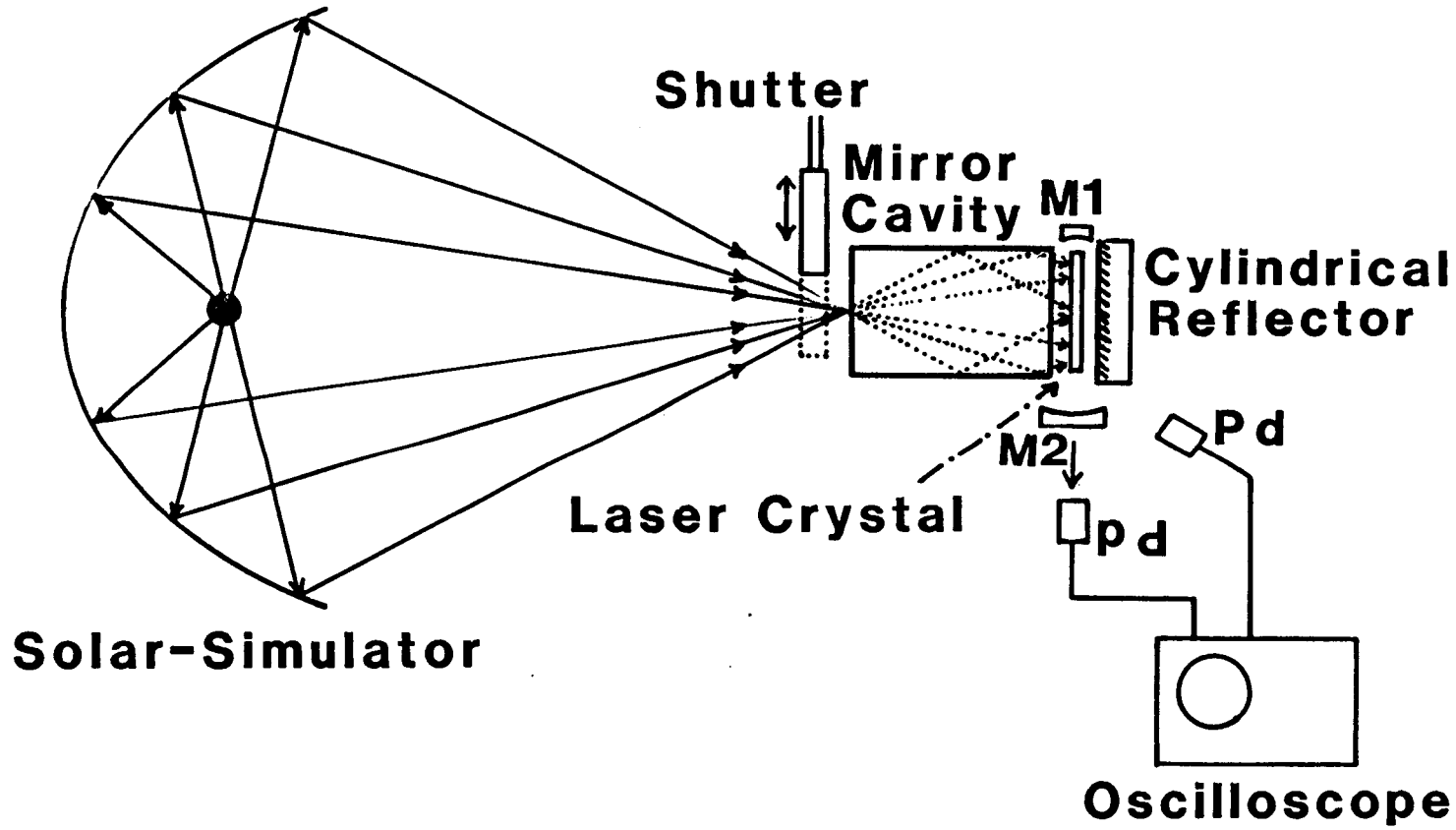

Figure 12. The Setup for the solar-simulator pumped solid state laser experiments with a mirror cavity to collect the solar-simulator's beam. M:mirror, Pd:silicon photodiode.

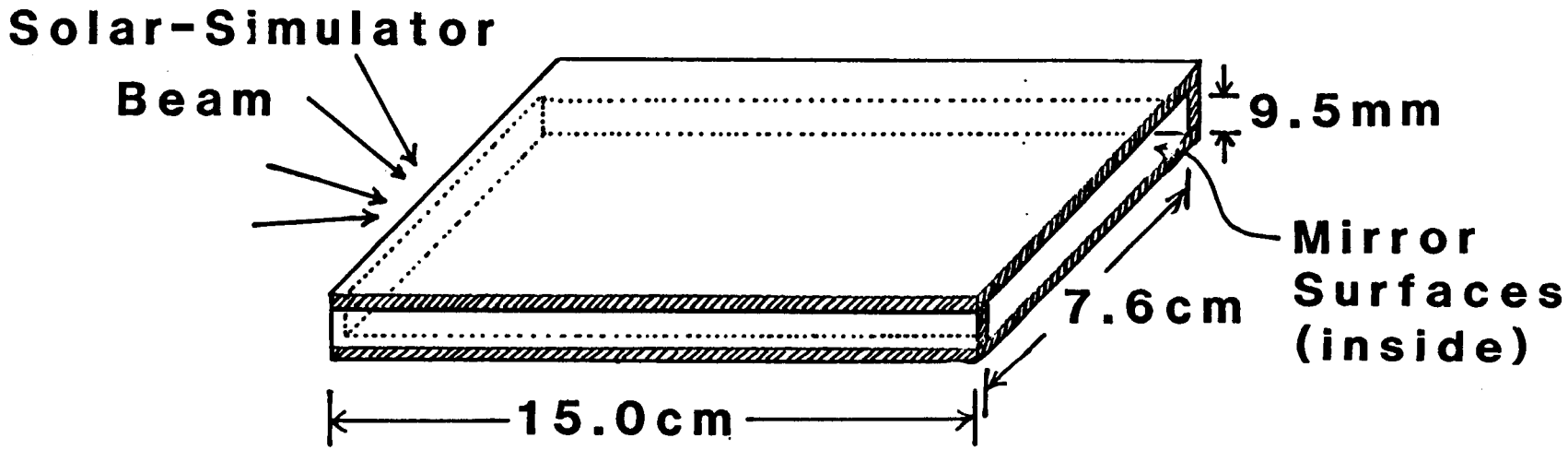

Figure 13. The shape and dimensions of the rectangular-type mirror cavity used to collect the solar-simulator beam on the laser crystal.

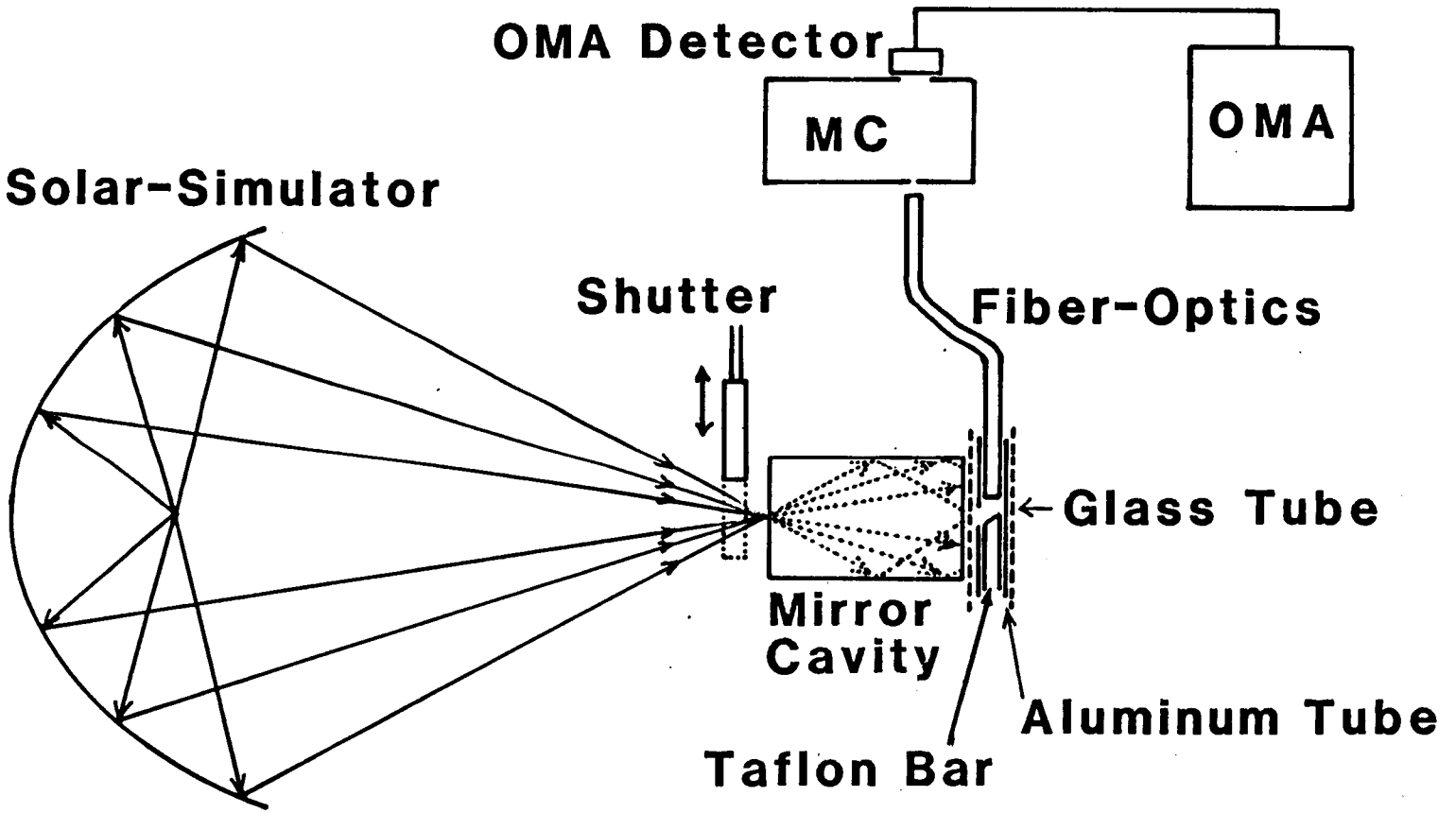

Figure 14. The Setup for the solar-simulator's beam intensity distribution measurement at the back of the mirror-cavity type beam collector. MC:monochromator, OMA:optical multichannel analyzer.

Fig. 15 shows the burn patterns taken at the back of the mirror cavity by placing a thermal paper in stead of the taflon reflector and aluminum tube. The upper burn pattern was taken at a distance of 1.0cm from the back of a 15cm long, 9.5mm thick and 7.6cm wide mirror cavity, and the lower one was taken in the same manner with a 16.6cm long, 6.5mm thick and 7.3cm wide mirror cavity. Figs. 16 and 17 show the intensity distributions of the solar-simulator beam at the back of the two types of miror cavity, respectively. The solid lines in the Figures were taken without any glass tube which is shown in Fig.14, but the dotted line of Fig. 16 was taken with use of a slightly diffused glass tube of 13mm I.D.. The uniformity of the solar-simulator's beam intensities at the back of the two mirror cavities was not perfect, but better than that at the cone axis of the conical collector in Fig. 1 which was reported in the previous semiannual progress report[Ref.1]. The measured solar-simulator's beam intensity at the center of the rear opening of the 15cm-long mirror cavity is shown in Fig. 18 as a function of the solar-simulator's input current. It was also observed that the peak intensity of the 15cm-long mirror cavity is a little higher than that of the 16.6cm-long mirror cavity, and the uniformity of the intensity with the former cavity is better than that of the latter one. The use of the slightly diffused glass did not improve the uniformity of the intensity distribution as shown in Fig. 16. The computed solar-simulator beam traces in the mirror cavities are shown in Figs. 19 and 20, respectively. The measured value of the divergence angle of the central peak line was about 17.6 degree from the center of the incoming beam.

Fig. 21 shows the laser signals of a Nd:YAG crystal measured with the experimental setup shown in Fig. 12. The crystal size was 1/8" diameter and 3" long, and it has anti-reflection coatings (@λ=1.06um) at both ends. Only pulsed operation has been tried beacuse the miror cavity was made of glass mirror and had no cooling device. The data was taken at the solar-simulator's input current of 600A. It was observed that the threshold electrical input power of the Nd:YAG laser with this mirror cavity geometry was higher than that with the cone geometry. This result can be also deduced from the solar-simulator beam intensity measurements which tells that the peak intensity with the mirror cavity at the solar-simulator input current of 200A was about

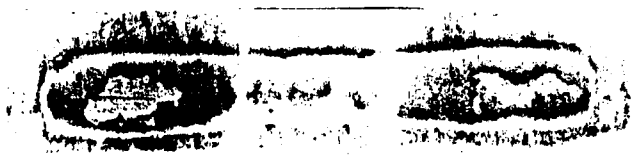

15.0cm-long Mirror Cavity

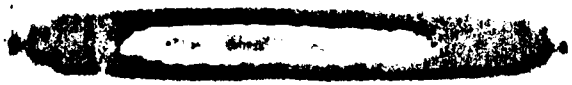

16.6cm-long Mirror Cavity

Figure 15. Burn patterns taken behind the two different mirror cavities.

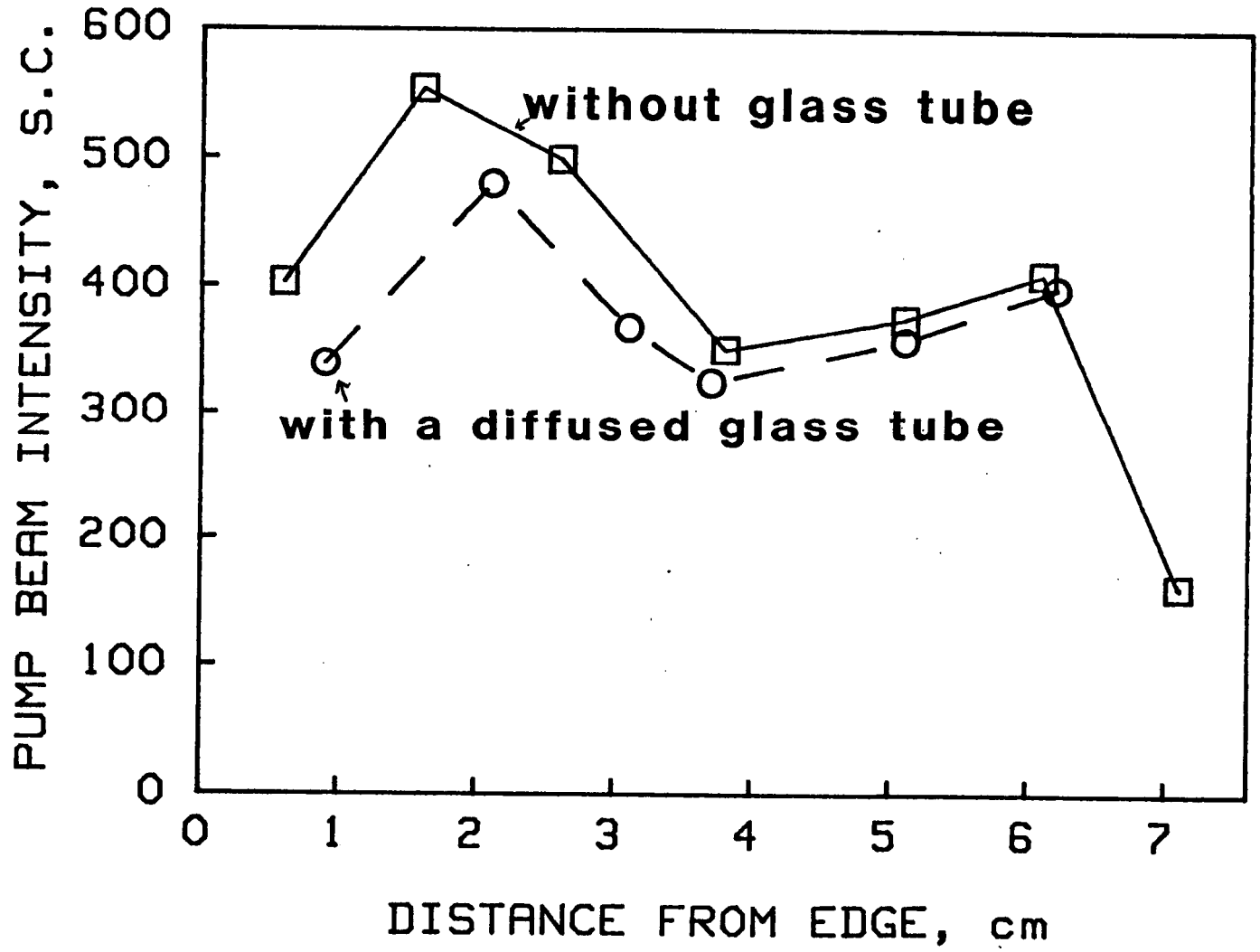

Figure 16. The intensity distribution of the solar-simulator beam at the back of the 15.0-cm long mirror cavity.

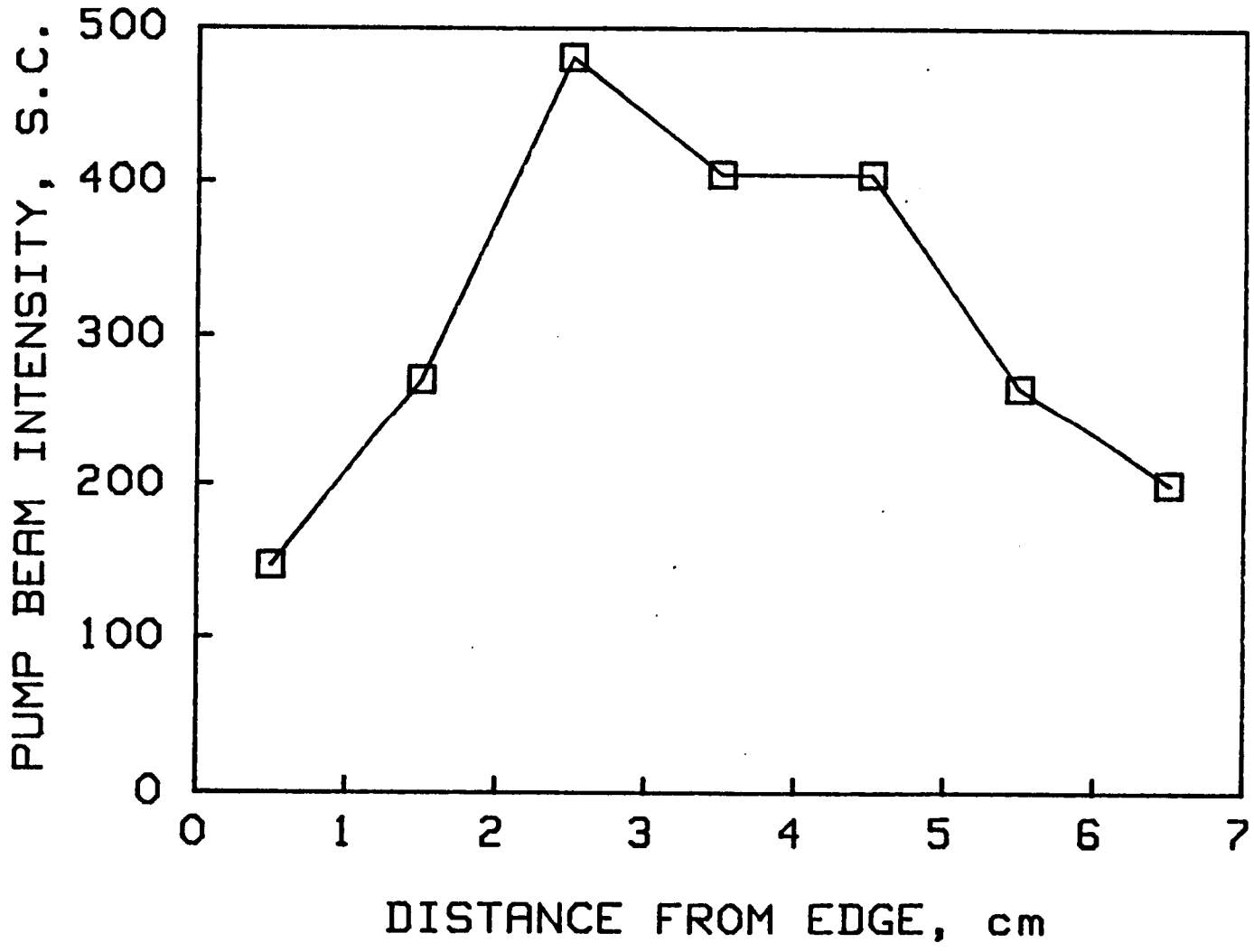

Figure 17. The intensity distribution of the solar-simulator beam at the back of the 16.6-cm long mirror cavity.

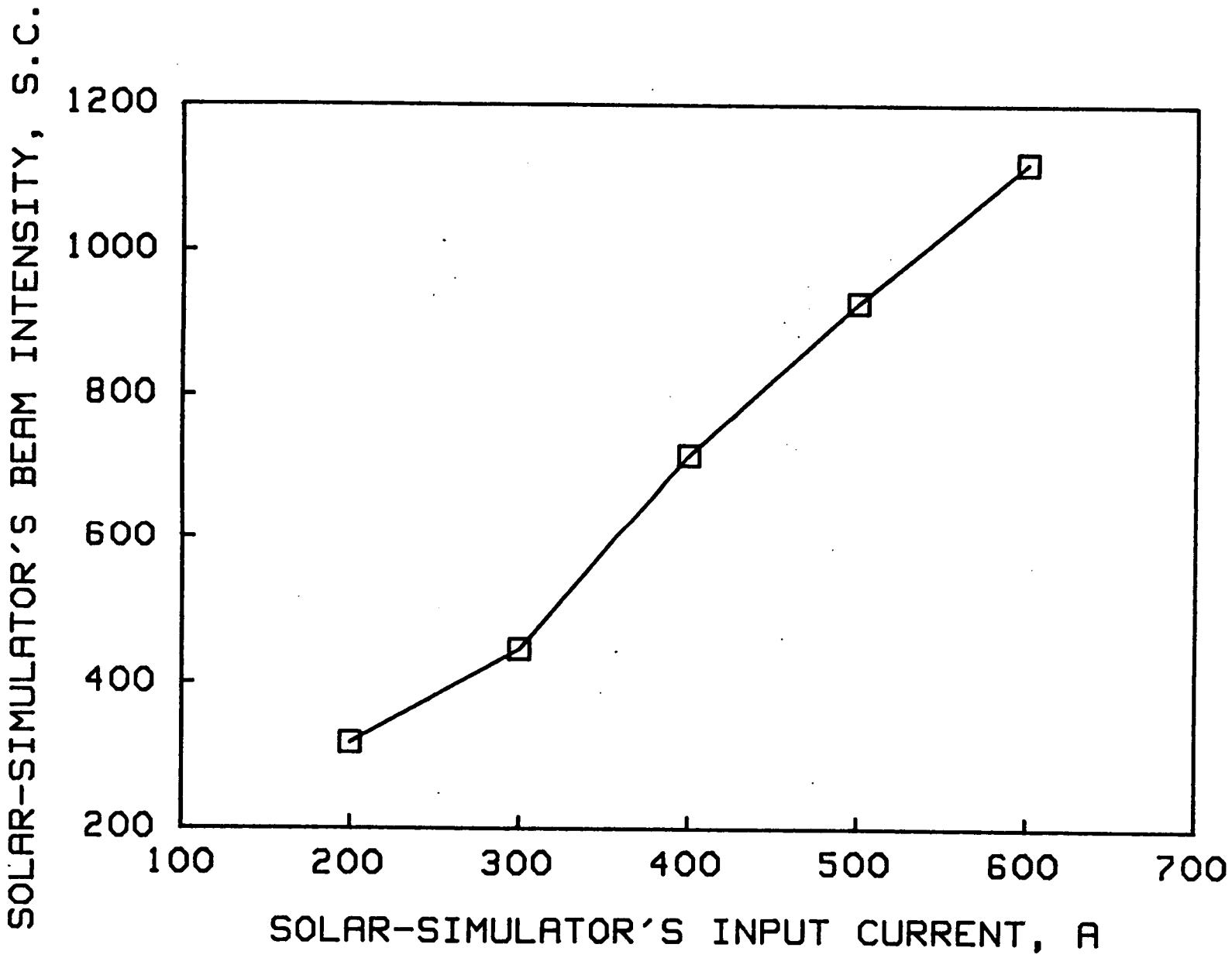

Figure 18. The solar-simulator's beam intensity at the center of the rear opening of the 15.0-cm long miror cavity as a function of the solar-simulator's input curent.

Figure 19. The computed solar-simulator's beam traces in the 15.0-cm long mirror cavity.

Figure 20. The computed solar-simulator's beam traces in the 16.6-cm long mirror cavity.

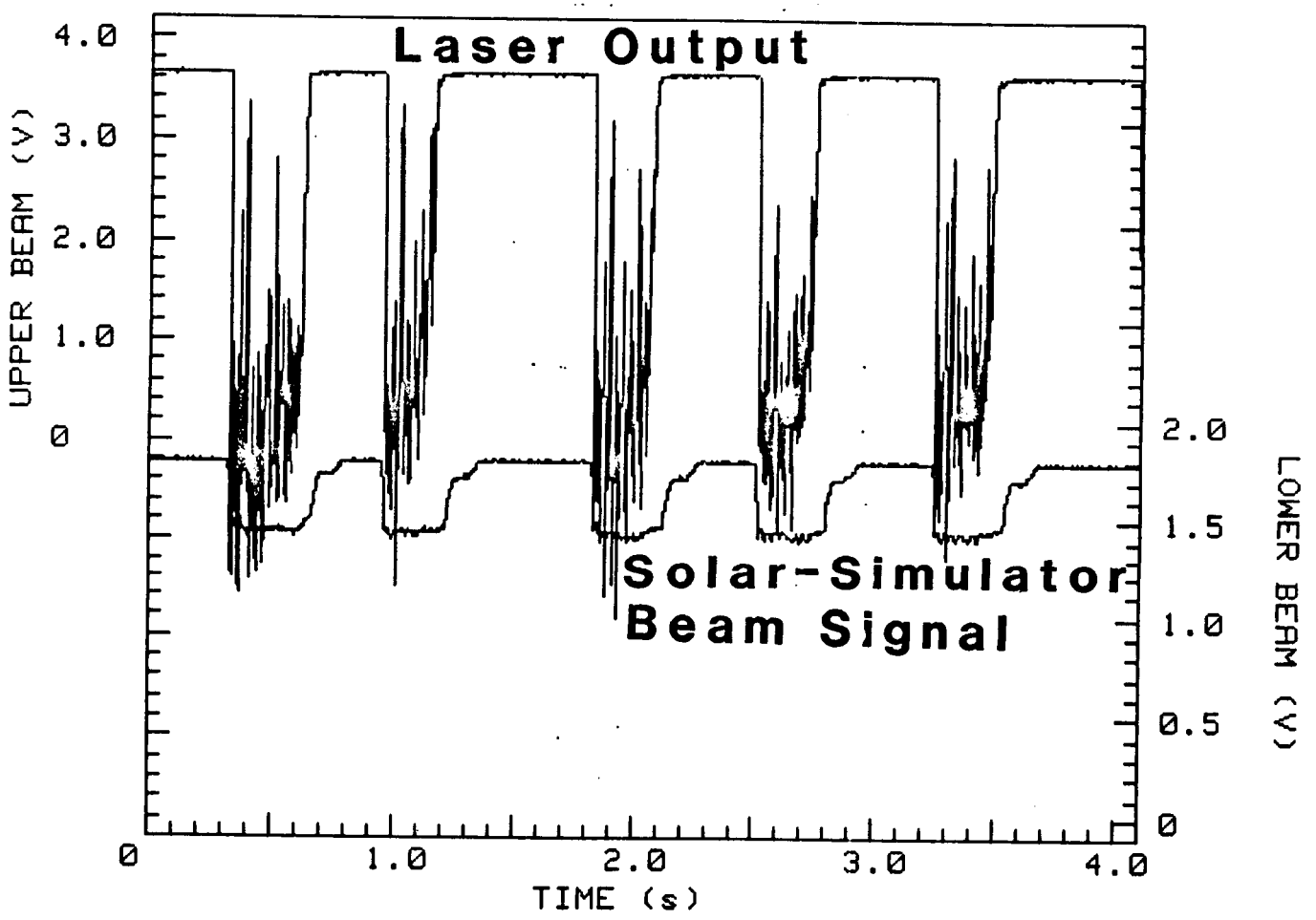

Figure 21. The observed Nd:YAG laser output and solar-simulator's beam signals using the experimental setup with the mirror cavity.

600 solar constants while that with the conical collector was about 1,000 solar constants. However, the optical threshold power density, which was observed to be about 1,000 solar constants within the experimental error range shown in Fig. 7, was about the same in both the mirror-cavity and cone geometries. The threshold can be lower by using an optimum output mirror coupling and an optimum alignment. As shown in Fig. 21, the laser beam intensity is quite stable in the consecutive pulses even though the intensity drops a little bit at the end of each pulse. Once a new water-cooled mirror cavity is ready, the cw laser operation will be attempted.

C. Conclusion

The Nd:YAG and Nd:Cr:GSGG crystals were tested for the solar-simulator pumped cw laser. The threshold pump-beam intensity for a 1/8" dia. x 3" long Nd:YAG crystal with 1 atomic doping was observed to be about 1,000 solar constants with mirror coupling of R1>99.5% and R2=98% both with 0.3-m curvature. The peak laser power of about 320mW and maximum lasing period of 15 seconds were observed from the Nd:YAG crystal.

CW laser operation of Nd:Cr:GSGG crystal was found to be very difficult from our measurement. The maximum lasing period observed was about 3 seconds under continuous solar-simulator pumping. Laser operation with continuously chopped-pumping has been also attempted, and more than 3 minute operation was achieved with the chopper's open-to-closed ratio of one to one. The peak laser power observed was 400 mW with a 1/8"-diameter x 2.94"-long Nd:Cr:GSGG crystal of the doping concentration of $2x10^{20}$ ions/cm of both Nd^{3+}- and Cr^{3+}-ions.

Finally, it was shown that the mirror-cavity type solar-simulator beam collector provided less intense beam collection than the conical collector, but the former provided more uniform beam collection than the latter. Another advantage of the mirror cavity was to remove thermal effect on the laser mirrors.

During this research period, only the two kinds of crystal were available. Bwt we expect that more crystals, which include a Nd:YAG with totally reflective mirror coating at one end, and 3 Nd:YLF crystals at various shapes and sizes, will be ready in the following project period. During the following period the optimum resonator condition for each laser crystal will be determined to improve the laser powers and to achieve stable cw laser operation. Threshold pump power, slope efficiency and thermal effect of the crystals will be also studied, and then the comparison of the 3 crystals will be made to determine the best candidate for the solar-pumped high power laser.

D. References

1. K. S. Han, K. H. Kim and L. V. Stock, "Direct Solar-Pumped Iodine Laser Amplifier," Semiannual Progress Report, NASA Grant No. NAG-1-441, March (1987)

2. S. E. Stokowski, "Nd:Cr:GSGG, will it replace Nd:YAG?," SPIE Vol.736 New Slab and Solid State Laser Technologies and Applictions, 22 (1987)

3. N. P. Barnes, D. J. Gettemy, L. Esterowitz, and R. E. Allen, "Comparison of Nd 1.06 and 1.33 um Operation in Various Hosts," IEEE J. Quantum Electron. QE-23(9), 1434(1987)

A KINETIC MODEL FOR A SOLAR-PUMPED IODINE LASER

Good agreement between the theoretical predictions and the experimental data is found for a flashlamp-pumped iodine laser for different fill pressures and different lasants ($i\text{-}C_3F_7I$, $n\text{-}C_4F_9I$, and $t\text{-}C_4F_9I$). The following loss mechanisms of the laser output power have been identified: a relatively large amount of initial molecular iodine in the fill gas and laser light scattering as a function of pressure.

A kinetic model has been constructed[1,2] to describe the kinetics of a solar-pumped iodine laser. Present kinetic coefficients are given in Table I. The kinetic model as it develops will be used to establish scalability of a solar-pumped iodine laser used in space for the generation and transmission of power. Recent experiments[3] are examined to further refine and develop the kinetic model.

The iodine laser experiments used an elliptical collector with the flashlamp and the laser tube at the foci. The flashlamp and the laser tube radii are .35 cm, the pumping length is 30.5 cm, and the distance between the mirrors is 60 cm with a two percent output mirror transmission. The pumping pulse had a gaussian shape with FWHM of one-half a millisecond. The peak power output of the flashlamp approximates that of a 7000 K blackbody radiator. The laser tube is first evacuated to about 10^{-6} torr and then the lasant is allowed to evaporate into the laser cavity until the desired pressure is reached. The static gas is then immediately pumped by the flashlamp. Care was taken to ensure a repeatable laser output.

The coupling of the flashlamp to the laser tube has been accurately modeled. The power output is calculated yielding the time of laser threshold, the energy output, and the lasing time. These output parameters are compared to the experimental data for the three gases in figures 1-3. In order to understand the experimental data, an initial condition (Table II) of a relatively large amount of molecular iodine $[I_2]_0$ is added in the kinetic model as a function of fill pressure. I_2 is observed as a discoloration of the lasant used to fill the laser tube. In addition to the $[I_2]_0$ the optical time constant[1] in the kinetic model is modified to incorporate a constant α_i as $\tau_c / (1 + \alpha_i P_0)$ becoming a linear function of the fill pressure P_0. This constant α_i is added to simulate the scattering of laser light by deposits on the Brewster windows and aerosols produced in the lasant. Varying these two parameters and the rate coefficients within known experimentally defined bounds [2,4] by using gradient search methods to minimize the differences between experimental data and theoretical predictions, there is reasonable agreement. For instance, at 25 torr less than a 6 percent difference between the theoretical calculations and the experimental data for the energy output of the laser for the three gases is found using the parameters given in tables I and II. This is well within the experimental reproducability given as $\pm$ 1 mJ/cm^2 for pressures less than 10 torr and $\pm$ 5 mJ/cm^2 for pressures greater than 15 torr.

In table II $[I_2]_0$ is compared to $[I_2]$ after equilibrium is reached $[I_2]_f$. For the lasants i-C_3F_7I and n-C_4F_9I the $[I_2]_f$ is significantly higher than $[I_2]_0$ (table II). Since I_2 is a strong quencher it can be expected, therefore, that the energy output will

also drop significantly if the lasant is repeatedly pumped without refilling; this is verified experimentally[3]. On the other hand, $[I_2]_f$ for t-C_4F_9I is not significantly greater than $[I_2]_0$ implying a repeatability of the output energy from multiple pulses of the same fill gas, and this is found experimentally. Furthermore, theoretically it is predicted that I_2 quenches the laser action in the gases i-C_3F_7I and n-C_4F_9I which is indicated by shorter lasing times for different pressures (figures 1, 2, and 3), as opposed to the longer lasing times of t-C_4F_9I. Longer lasing times and subsequent higher energy outputs of t-C_4F_9I are primarily due to the smaller recombination rate K_3 which forms the dymer R_2 (table I) since it allows the free radical to recombine with iodine creating the parent gas rather than I_2. These properties - slow I_2 and R_2 formation - make the lasant t-C_4F_9I a good candidate for a space-based solar-pumped laser.

Good agreement between the theoretical model and the experimental data for this system has been reached. The results are generally within experimental reproducibility. The reaction rate coefficients given here represent the best value obtainable within the context of this experimental system and are within the range of known uncertainties. The development of the kinetic model represents a continuing effort to establish the scalability of a solar-pumped space-based iodine laser to be used for the transmission and generation of power.

REFERENCES

1. L. V. Stock, J. W. Wilson, and R. J. De Young,"A Model for the Kinetics of a Solar-Pumped Long Path Laser Experiment," NASA TM 87668, May 1986.

2. J. W. Wilson, S. Raju, and Y. J. Shiu, "Solar-Simulator-Pumped Atomic Iodine Laser Kinetics," NASA TP 2182, August 1983.

3. Ja H. Lee, W. R. Weaver, and B. M. Tabibi, "Characteristics of t - Perfluorobutyl Iodide as a Solar-Pumped Laser Material." Conference on Lasers and Electro-optics, May 1985.

4. J. W. Wilson et al., "Threshold Kinetics of a Solar-Simulator-Pumped Iodine Laser," NASA TP 2201, 1984.

TABLE I - REACTION RATE COEFFICIENTS FOUND WITHIN PUBLISHED VALUES.

[Along with the value found for α_i (See Text)]

Reactions	Symbol	Reaction Rate Coefficients, $(cm^3)^n/sec$		
		R = i-C_3F_7	R = n-C_4F_9	R = t-C_4F_9
$I^*+R \rightarrow RI$	K1	$.163\times10^{-11}$	$.749\times10^{-12}$	$.956\times10^{-12}$
$I+R \rightarrow RI$	K2	$.133\times10^{-10}$	$.988\times10^{-11}$	$.705\times10^{-11}$
$R+R \rightarrow R_2$	K3	$.438\times10^{-11}$	$.606\times10^{-11}$	$.222\times10^{-13}$
$R+RI \rightarrow R_2+I$	K4	$.766\times10^{-16}$	$.776\times10^{-16}$	$.475\times10^{-16}$
$I_2+R \rightarrow RI+I$	K5	$.178\times10^{-11}$	$.224\times10^{-10}$	$.111\times10^{-11}$
$I^*+RI \rightarrow I+RI$	Q1	$.112\times10^{-15}$	$.660\times10^{-15}$	$.923\times10^{-15}$
$I^*+I_2 \rightarrow I+I_2$	Q2	$.339\times10^{-10}$	$.339\times10^{-10}$	$.339\times10^{-10}$
$I^*+I+RI \rightarrow I_2+RI$	C1	$.109\times10^{-32}$	$.868\times10^{-33}$	$.363\times10^{-32}$
$I+I+RI \rightarrow I_2+RI$	C2	$.597\times10^{-31}$	$.218\times10^{-31}$	$.420\times10^{-31}$
$I^*+I+I_2 \rightarrow 2I_2$	C3	$.800\times10^{-31}$	$.800\times10^{-31}$	$.800\times10^{-31}$
$I^*I+I_2 \rightarrow 2I_2$	C4	$.393\times10^{-29}$	$.393\times10^{-29}$	$.393\times10^{-29}$
	α_i	$.339\times10^{-1}$	$.262\times10^{-1}$	$.77\times10^{-2}$

TABLE II - INITIAL I_2 DENSITY $[I_2]_0$ AND I_2 DENSITY AFTER EQUILIBRIUM IS REACHED IN THE LASER TUBE $[I_2]_f$. FOR DIFFERENT PRESSURES AND LASANTS.

LASANTS	i - C_3F_7I (x 10^{15})		n - C_4F_9I (x 10^{15})		t - C_4F_9I (x 10^{15})	
Pressure (torr)	$[I_2]_0$ (molec/cm^3)	$[I_2]_f$	$[I_2]_0$ (molec/cm^3)	$[I_2]_f$	$[I_2]_0$ (molec/cm^3)	$[I_2]_f$
5.	.42	2.23	.41	2.43	.41	.31
10.	.41	3.80	.40	4.30	.40	.48
15.	.42	5.17	.41	5.91	.41	.63
20.	.43	6.34	.42	7.18	.42	.79
25.	.46	7.39	.45	7.81	.45	.95
30.	.49	8.31	.48	9.86	.48	1.12
40.	.59	9.60	.57	12.06	.58	1.49

IODINE LASER KINETICS

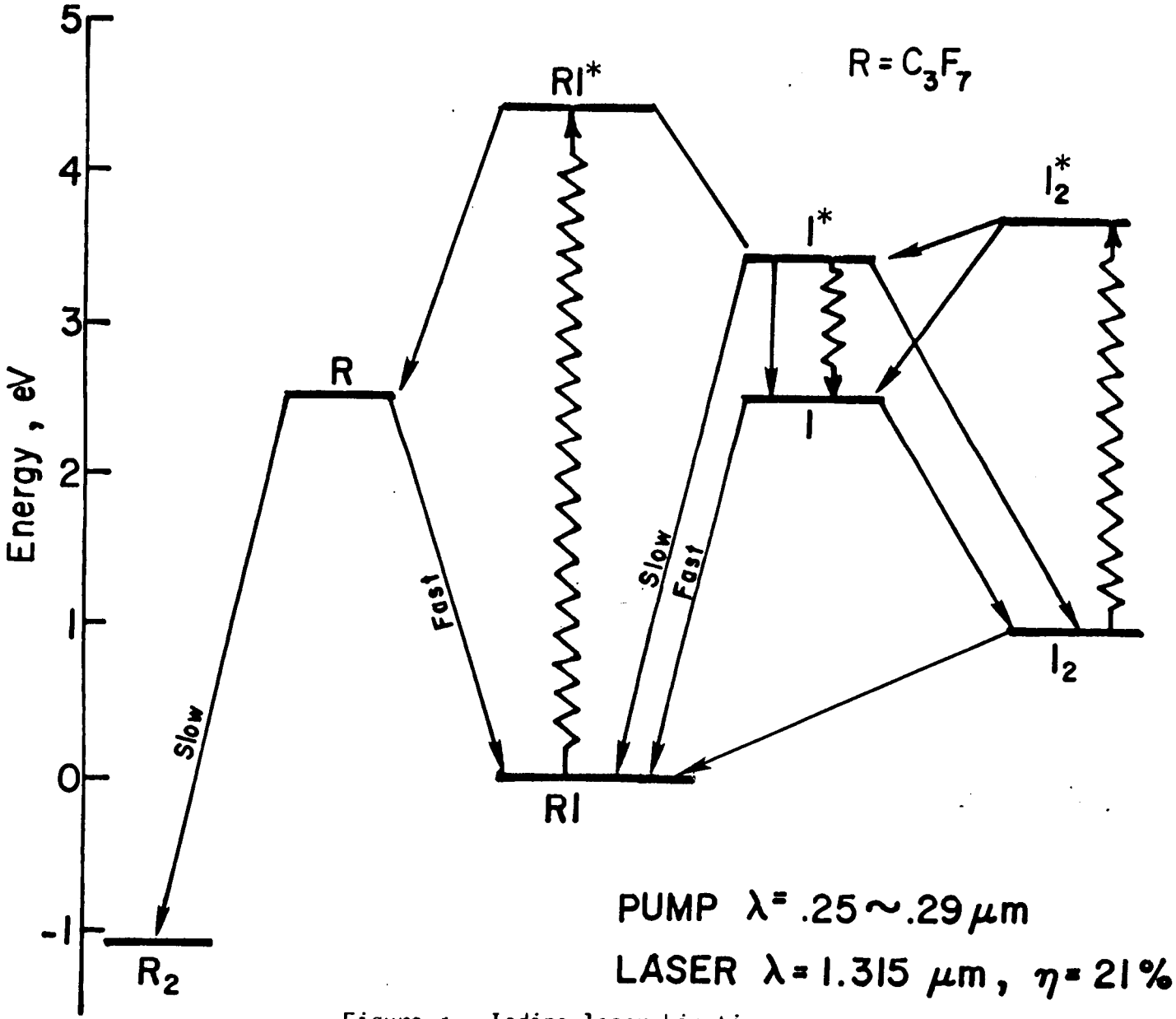

Figure 1.- Iodine laser kinetics.

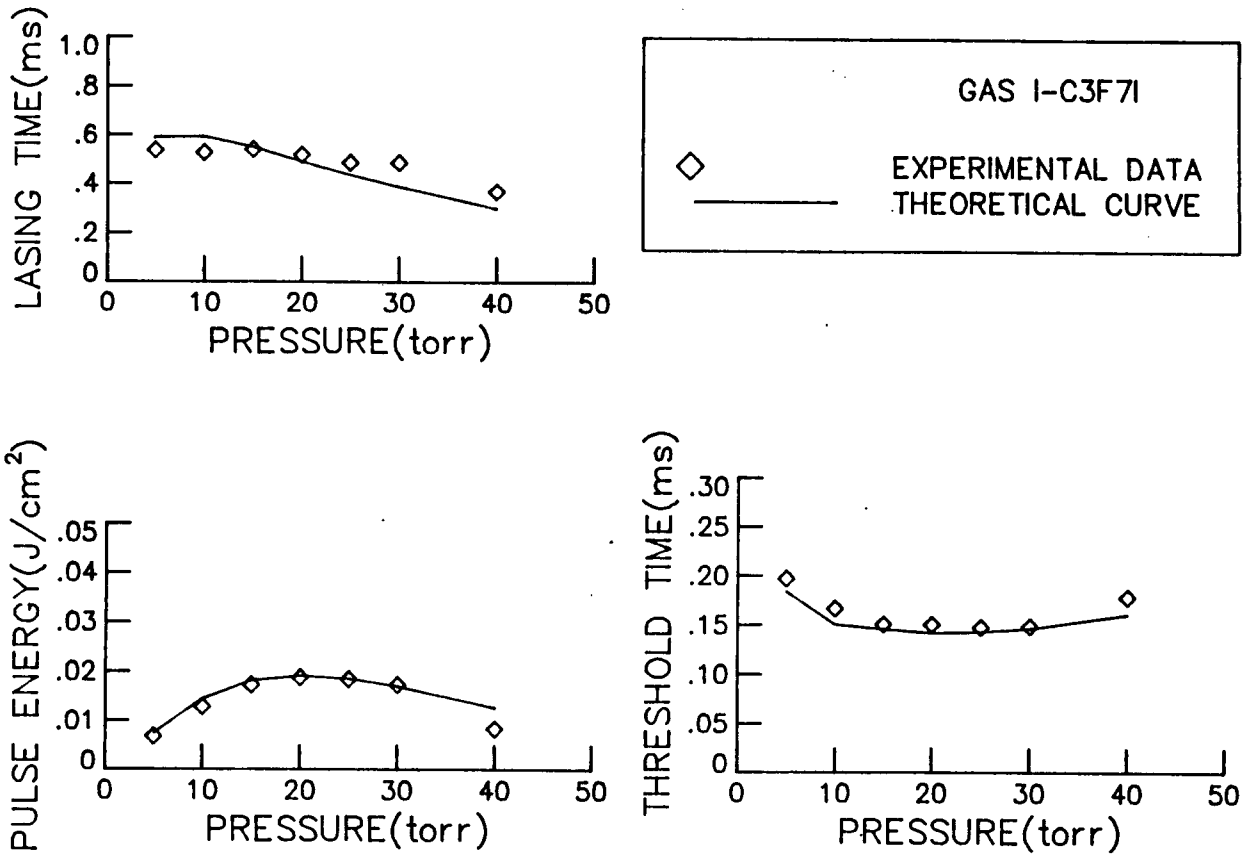

Figure 2 -- Experimental data and theoretical predictions for the lasant i-C_3F_7I.

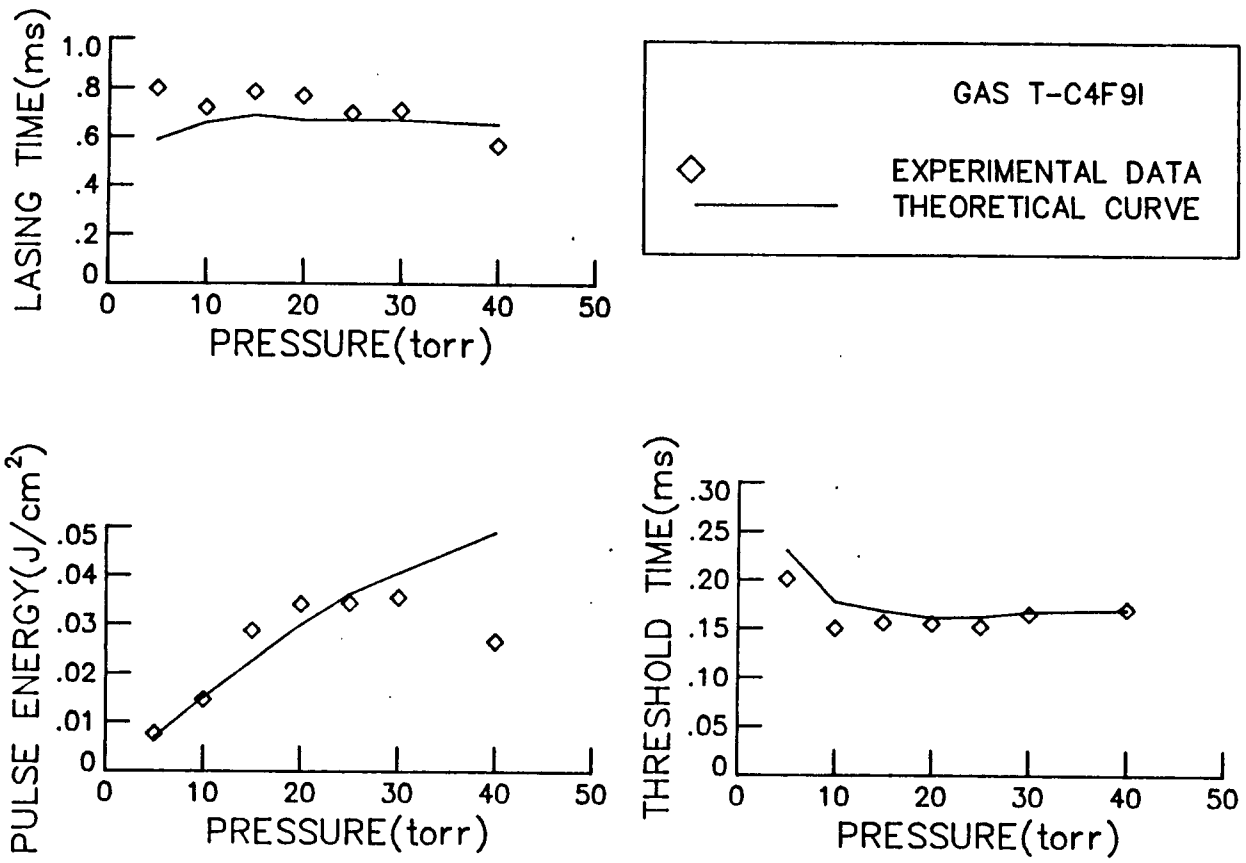

Figure 3 -- Experimental data and theoretical predictions for the lasant t-C_4F_9I.

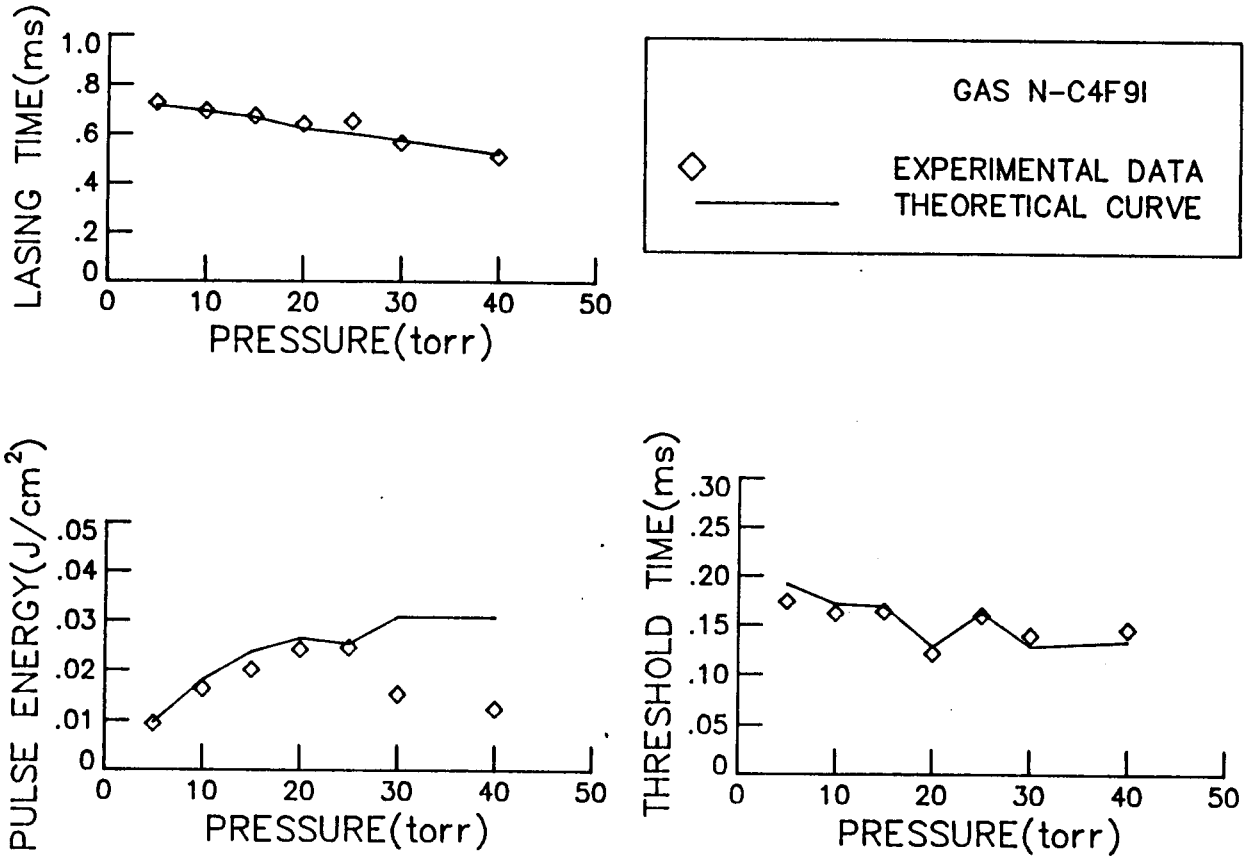

Figure 4 -- Experimental data and theoretical predictions for the lasant n-C_4F_9I.